Molecular Dynamics Simulations for Melting of Palladium Nanoclusters and Nanowires

Ling Miao, Venkat R. Bhethanabotla*T and Babu Joseph
Chemical Engineering Department, University of South Florida, Tampa, Florida, 33620, USA

We present results from a molecular dynamics simulation study of a Pd cluster and a nanowire, both of 2.3 nm diameter, using the Sutton_Chen manybody potential function. Changes in thermodynamic and structural properties of these two systems during heating were studied. We found that the melting temperature of the Pd nanowire of 1200 K is lower than the simulated bulk value (1760 K) but higher than that of the cluster at 1090 K. Melting behaviors were characterized by a number of thermodynamic, structural and dynamical parameters. Surface pre-melting at much lower temperatures than the near first order transition temperatures noted above was observed in both Pd systems. The surface pre-melting temperature range was higher for the nanowire than for the cluster. Surface melting in nanowires manifests itself as large amplitude vibrations followed by free movement of atoms in the plane perpendicular to the nanowire axis, with axial movement arising at temperatures closer to the transition temperature. Increase in nanowire diameter as well as shape change are seen to result from this axial mixing. Atomic distributions indicated that the nanowire could undergo mechanical instabilities and break upon heating. Bond order parameters indicated that the nanocluster retained the initial fcc structure, whereas, the nanowire tended towards the hcp structure. Simple melting theories could not explain the actual depression of the melting point in both systems.

1. Introduction

Studies of the melting process and thermodynamics properties of particles at nanometer length scales have attracted both theoretical[1,2] and experimental[3,4,5] interest because of their dramatically different behavior from bulk materials.[6] Transition and noble metal[7,8,9] or alloy[10,11] clusters and nanowires are getting more attention, mainly because their extensive applications in catalysts, electronic and opto-electronic nanodevices. Theoretical investigations of the melting behavior of clusters and nanowires have been mostly by means of Monte Carlo (MC) and Molecular Dynamics (MD) computer simulations and are focused on the followings aspects: (i) investigation of the melting temperature and thermal stability during the melting process;[12,13] (ii) the structural evolutions and mechanical properties during heating;[14] (iii) relationship of structural characteristics and size effects with temperature.[15,16] For example, Wang et.al. find that for Ti nanowires thinner than 1.2 nm, the coexistence mechanism of the solid and liquid state play a significant role in the melting process. Liu et.al.[17] observed three characteristic time periods, disordering and reordering, surface melting, and overall melting in golf isomers.

Clusters are often considered as a bridge between individual atoms and bulk material. Recent experimental and theoretical studies demonstrated that metallic nanowires have helical multi-walled cylindrical structures[18] which are different from those of bulk and clusters. However, at the same time, nanowires also have thermodynamic characteristics which are similar to either clusters or bulk, because of the large surface-to-volume ratio in these

nanostructures. Therefore, a comparison of clusters and nanowires can provide an opportunity to better understand their behavior.

In this paper, melting characteristics of palladium nanoclusters and nanowires of comparable size are compared. Pd has a number of potential applications in heterogeneous catalysis as well as microelectronic and optoelectronic devices. For example Pd nanoclusters and nanowires have been used widely in the design of high performance catalysts[19,20] and nanoscale electronic devices, such as chemical sensors.[21,22,23] Several experiments clearly indicate that quantum behavior of metal nanoclusters is observable, and is most strongly expressed between 1 and 2 nanometers, therefore, particles in that size region should be of most interest.[24] For example, Volokitin found that 2.2 nm Pd clusters show the most significant deviations from bulk behavior at very low temperatures compared with those of 3.0, 3.6 and 15nm.[25] Simulation study of Pd nanomaterial provides an opportunity for further understanding its unique role in experimental phenomena. Although the size of the metallic clusters being studied in the literature ranged from tens to several thousand atoms, most efforts have been focused on sizes below 150 atoms for both Pd[26] and other metals. To facilitate comparison with experimental data, we investigate both melting and structural behavior of a 2.3 nm Pd cluster with 456 atoms and comparable sized nanowire with 1568 atoms, also of 2.3 nm diameter.

2. Simulation details

2.1 Potential model

Because of the delocalized electrons in metals, the potential functions, which describe the interactions of particles, should account for the repulsive interaction between atomic cores as well as the cohesive force due to the local electron density. The Sutton_Chen (S_C) potential[27] is used in this paper to describe the interaction of various metals, such as Ag, Au, Ni, Cu, Pd, Pt, Pb. It is expressed as a summation over atomic positions:

$$U = \varepsilon_{pp} \sum \left(\frac{1}{2} \sum_{j \neq i}^{N} \left(\frac{\sigma_{pp}}{r_{ij}} \right)^{n} - c\sqrt{\rho_i} \right), \tag{1}$$

where $\rho_i = \sum_{j \neq i}^{N} \left(\frac{\sigma_{pp}}{r_{ij}} \right)^{m}$ is a measure of the local particle density. Here r_{ij} is the separation distance between atoms, c is a dimensionless parameter, ε_{pp} is the energy parameter, σ_{pp} is the lattice constant, and m and n are positive integers with $n>m$. The first term of the expression is a pair-wise repulsive potential, and the second term represents the metallic bonding energy between atomic cores due to the surrounding electrons. This potential can reproduce bulk properties with remarkable accuracy.[28] It provides a reasonable description of small cluster properties for various transition and noble metals.[29,30] S_C potential has also been applied to model the interaction and study the properties of bimetallic alloys and metal/substrate systems.[11,31,32] Values of S_C parameters for Pd simulations in this paper were taken from the original work of Sutton and Chen[27] as listed in Table 1:

Table 1 Sutton_Chen potential parameters for Pd

σ (Å)	ε (10^{-3} eV)	C	n	m
3.8907	4.1790	108.27	12	7

2.2 Computational method

MD simulations were performed using the DL_POLY[33] package. The system was simulated under canonical (constant NVT) ensemble using the Verlet leapfrog algorithm.[34] Periodic boundary conditions were applied only on the axial direction of the nanowire. No boundary conditions were applied to the cluster. The bulk systems were studied with 3D periodic boundary conditions under constant pressure and temperature (NPT). Both cluster and nanowire were started from face-centered cubic Pd bulk, using spherical cutoff radii to get certain sized ball and cylindrical shapes. The radius of the cluster is defined as[35]

$$R_c = R_g \sqrt{5/3} + R_{Pd}\,, \tag{2}$$

Where the atom radius R_{Pd} =1.37A. R_g is the radius of gyration, given by

$$R_g{}^2 = \frac{1}{N}\sum_i \left(R_i - R_{cm}\right), \tag{3}$$

where R_i-R_{cm} is the distance from center to the coordination point. In all the simulations reported here, a time step of 0.001ps was used. The initial samples with atoms in ideal face centered cubic (fcc) positions were first relaxed by simple quenching to zero degree. Each system was then heated with a temperature step of 50 K. The step was decreased to 10 K when close to the transition temperature.

3. Results and discussion

3.1 Melting temperature

The temperature of melting transition can be identified in many ways. We first employ the variations of total potential energy and heat capacity during heating. They are shown in Figure 1. Potential energies increase linearly with temperature in the early stage, but deviate from the linear dotted lines at higher temperatures. These deviations, associated with surface melting phenomena, will be discussed later. When close to the transition temperature, simple jumps in total potential energy, indicative of near first order transitions, can be easily observed. The hysteresis loop bounded by the freezing and melting temperatures was found in both Pd cluster and nanowire (see Qi's[36] also).

According to the potential energy curve, we estimate the melting transition of Pd cluster to occur at 1090 K, and that of the Pd nanowire at 1200 K. Both temperatures are much lower than the bulk melting temperature of 1760 K (also obtained from simulation). This is because in the bulk system there are no heterogeneous nucleation sites, that a free surface or solid-liquid surface, can exhibit.

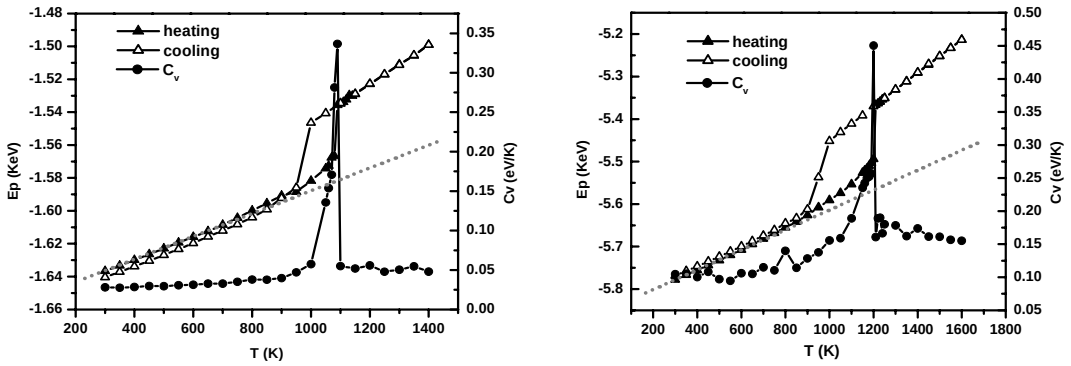

FIG. 1. Potential energy and heat capacity of a 2.3 nm diameter Pd (a) nanocluster (right) and Left (b) nanowire (left). (Heating and cooling curves match above melting point)

The constant-volume specific heat capacity C_v is calculated by a standard formula:

$$C_v = \frac{\left\langle \left(\delta E\right)^2 \right\rangle}{k_b T^2} = \frac{\left\langle E^2 \right\rangle - \left\langle E \right\rangle^2}{k_b T^2}, \qquad (4)$$

where E is total potential energy from the heating curve of Figure 1, k_b is the Boltzman constant, and T is the temperature. Melting point is defined as the temperature with the maximum apparent heat capacity. The C_v curves in Fig. 1(a) and 1(b) indicate the same melting temperatures as those from *Ep* curves. Compared to the C_v curve before melting for the Pd cluster, that of Pd nanowire shows more structure. We also observe a small upward jump in the nanowire heating curve, after which the slope increases quickly until the large jump appears. This deviation from linearity is a result of surface melting or surface reconstruction,[37] which implies that the melting process takes place in two stages, premelting and homogeneous melting. Even though this change is clearly visible from the plot for the Pd cluster, further characterization of the surface melting via dynamical variables such as the diffusion behavior and velocity auto-correlation functions revealed differences in the details of the premelting. These characterizations are discussed later in this paper. Based on the data shown in Figure 1, we can estimate the melting temperature to be 1090 K for the 2.3 nm Pd cluster, and 1200 K for the infinitely long nanowire.

3.2 Analysis of atomic motion

The structural features of the nanowire upon heating were further explored by visualization through snap shots and trajectory plots to understand the differences in the surface pre-melting phenomenon in the nanowire and cluster. Figure 2(a) shows sample projected coordinates, on to the plane parallel to the nanowire axis, of each atom at two temperatures of 700 K and 800 K, as blue and red dots, as well as the a dashed line connecting each of the atomic positions at the two temperatures. What is apparent is an oscillatory motion in the plane perpendicular to the nanowire axis, with atoms mostly retaining their positions through the simulation duration. Very few surface atoms exhibit large movement

along the wire axis, crossing different planes. This surface atomic movement was found to be rarer at temperatures lower than the 700–800 K shown in this figure. While a bit more difficult to see from Figure 2(b), similar behavior is exhibited at the slightly higher temperatures of 900 and 1000 K. The top view in Figure 2(b) shows more movement at the surface than towards the center of the wire, Analysis of these and similar plots along with trajectory visualizations have provided a picture of the surface pre-melting of one where the nanowire exhibits increasingly freer motion of the surface atoms in the plane perpendicular to the nanowire axis at temperatures much below the near first order transition temperature, with the degree of freedom parallel to the nanowire axis available at higher temperatures, closer to the transition temperature. The surface pre-melting is further characterized by a shrinking solid-like core of the nanowire, as the temperature increases to the transition point. This physical picture is consistent with the deviation of the potential energy curve from linearity as shown in Figure 1(b), however, these details of the structural and dynamical changes are not apparent from that plot. Indeed, the potential energy curve for the near spherical nanocluster shown in Figure 1(a) exhibits similar behavior, however, details of the surface pre-melting are quite different, a difference arising from the difference in the geometry. It should be noted here that both nanoclusters and nanowires of various metals have been synthesized by a variety of templating and other solution techniques, and it is possible to observe these differences in melting behavior upon heating of these nanomaterials. No such experiments have been reported in the literature to our knowledge.

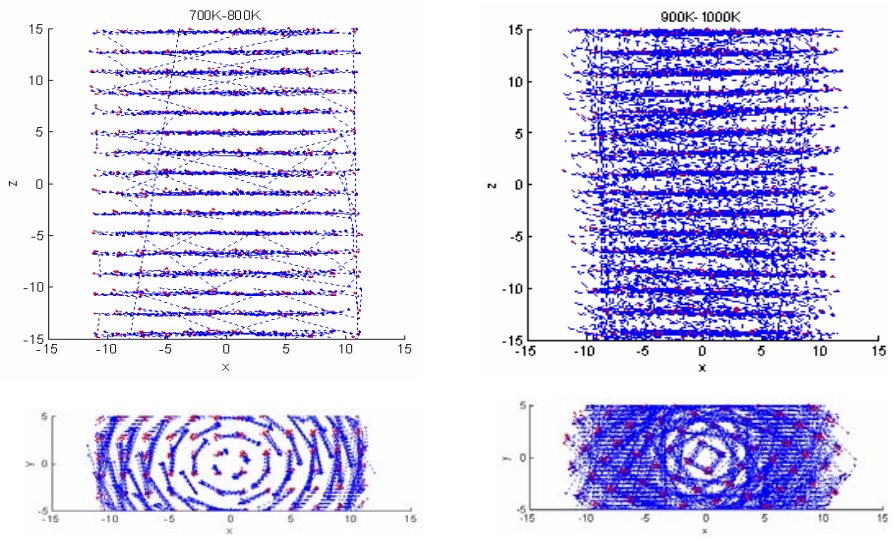

(a) **(b)**

FIG. 2. Snapshots of equilibrated atomic positions, shown as projected coordinates in planes parallel (upper) and perpendicular (down) to (a) the nanowire axis. Blue dots are for 700 K and red dots are for 800 K, with the blue dashed lines connecting the same atoms at the two temperatures. Similar plot for (b) 900 K and 1000 K.

Components of the velocity auto-correlation function in cylindrical coordinates were calculated as functions of distance from the nanowire axis to characterize atomic motion in the surface pre-melting regime. v_θ and v_z characterize movement in the *x*-*y* plane and in the *z* direction. Figure 3 shows the correlation of v_θ, and v_z with time at 800 K. The five curves in

both plots represent correlated atoms at different distances from the center with 1 being the closest and 5 the farthest. The wire was partitioned into these 5 shells with *dR*=2.77Å based on the initial equilibrium atomic positions (time origins of the time-correlation function calculations), chosen to be close to the interatomic distance in bulk solid Pd of about *2.75 Å*. Atoms stayed within their shells for the duration of the correlation time, and beyond, justifying these calculations to further understand the surface melting phenomenon.

Both components of the correlation functions for the inner shells exhibit rebounding oscillations that decay with time, indicative of localization at lattice sites. Comparing the two plots, v_θ has shorter correlation time and much larger depth of the minima than v_z, which implies larger amplitude tangential vibrations than axial. Behavior of atoms in the outer shells (especially, the outermost shell) is significantly different, at this temperature of 800 K, with surface premelting apparent. Nearly liquid-like motion is inferred from the single damped oscillation with one minimum before decorrelation with time.

While results at the one temperature of 800 K are shown in Figure 3 to illustrate the surface pre-melting phenomenon, v_θ and v_z calculated at other temperature corroborate the arguments developed here. At temperatures higher than 900 K, axial movement is larger while the tangential oscillations are dampened. The wire diameter increases with temperature as a result of these movements.

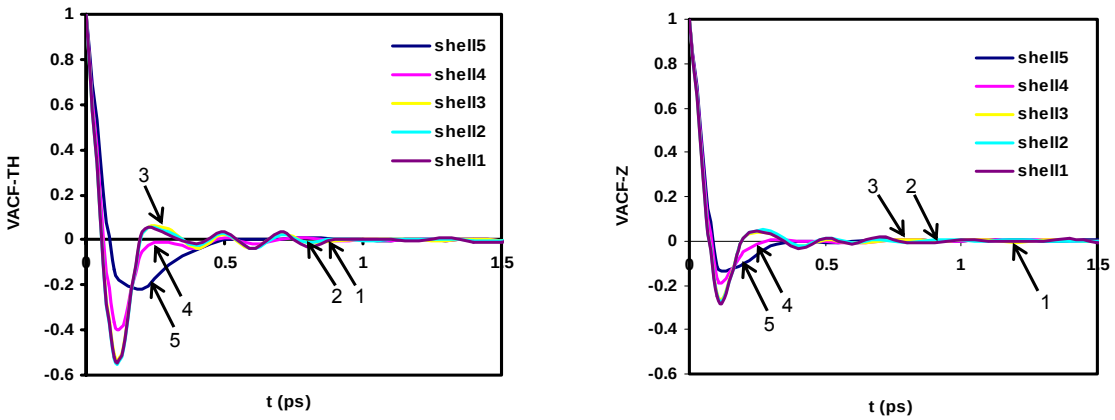

(a) **(b)**

Fig. 3. Velocity autocorrelation functions for atoms in different shells at increasing distance from the center of the Pd nanowire at 800 K. Shell 1 is the closest to the wire axis and shell 5 is the farthest. (a) v_θ and (b) v_z

3.3 Surface melting

Surface melting is observed frequently in simulations of nanoparticles. Surface atoms melt at temperatures below the transition temperature, and then the quasi-liquid skin continuously grows thicker as the temperature increases. The inner regions stay ordered until the transition temperature. The temperature at which the film thickness diverges to infinity is thought of as the bulk melting point. For ultra thin gold nanowires, Wang et.al. found the

interior melting temperature to be lower than that of the surface, indicate that the melting actually starts from inside, exhibiting no surface melting behavior.

Snapshots of atomic positions projected on to a plane (perpendicular to the axis in the nanowire case) are shown in Figure 4. These provide evidence for surface melting in both the Pd cluster and nanowire cases.

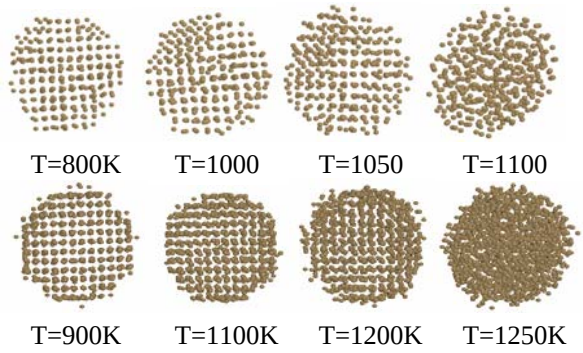

FIG. 4. Snapshots of the projected atomic positions of (a) the 456 Pd atom clusters (top) and (b) the 1568 atom Pd nanowire (bottom) projected to a x-y plane at different temperatures.

Further evidence of surface melting in both cluster and wire is obtained from self diffusion coefficients calculated as functions of radial distance using mean square displacements. As in the calculation of the velocity auto-correlation functions, the atoms were assigned to bins based on their initial positions at the end of the equilibration period. The mean square displacements for each shell were then generated by averaging over a 25 ps trajectory with sampling done every 0.1 ps. Averages taken over 25 ps trajectory with different origins gave the same result which is indicative of a system that is truly in equilibrium. The self-diffusion coefficients were calculated for each radial shell at various temperatures using the equation:

$$D = \frac{1}{6N} \lim_{t\to\infty} \frac{d}{dt} \sum_i \left[r_i(t) - r_i(0) \right]^2 \qquad (5)$$

These are shown in Figure 5. In all the cases, we find the diffusivities of outer shells to be higher than those of the inner ones. If $D_1 - D_5$ denote self-diffusion coefficients of these shells from inner to outer, we found that at lower temperatures, both clusters and nanowires have similar self-diffusion coefficients of the order of 10^{-3} Å ^{2}/ps. Atoms in the outer shells have larger diffusion coefficient than the atoms closer to the core atoms. As the temperature further increases, the diffusion coefficient on the outermost shell, D_5, first starts to increase rapidly. This is followed by.D_4. While D_1, D_2, D_3 retain their values from the lower temperatures. This state is maintained until the melting transition temperatures are approached. The larger diffusion coefficients in outer shells and relatively static state of inner shells at temperatures below the transition temperatures supports the existence of surface melting in both Pd cluster and nanowire. Atoms on the surface have weaker restraining forces than the core atoms. Although surface melting in some sense is not necessarily a diffusive process, it can be considered a complex phenomenon involving cooperative motion. According to the Lindemann criterion, the phase transition occurs when atomic motion exceeds 10-15% of interatomic distance. From the variation of the diffusion coefficients in various bins, we can infer a

continuous layer-by-layer melting as the atomic displacements meet the Lindemann criterion in a layer-by-layer manner, until, the criterion is met for the remaining solid core all at once, at the near first order transition temperature. From the diffusion plots, together with the variations of potential energies and heat capacity curves in Figure 1, we estimate the surface melting regions of the 2.3 nm Pd cluster and nanowire to be about 700-800K, and 800-900K, respectively. At melting points, diffusion coefficients of all the shells exhibit large jumps of similar magnitude, indicating the phase transitions from solid to liquid.

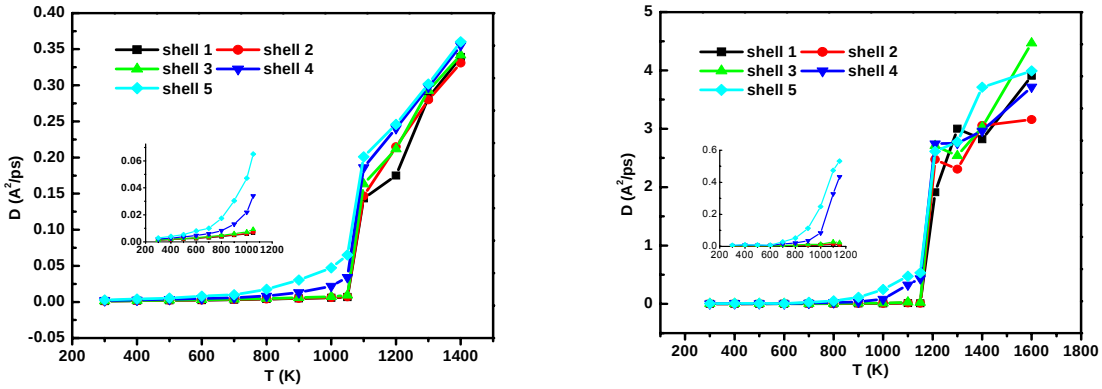

FIG 5. Self-diffusion coefficient for atoms in different radial shells at various temperatures of (a) Pd cluster and (b)Pd nanowire

3.4 Analysis of structural characteristics

Structural properties and changes in them during heating are of interest in understanding mechanical and catalytic properties of materials. Experimental observations include changes in the lattice parameter, surface coordinations and structural fluctuations. Some theoretical calculations include detailed studies of the topology and structural stability. Many small clusters, with special numbers of atoms, so-called magic numbers, have proven to be more stable than others.[38] The change in crystallographic structure can be attributed to surface energy. Icosahedral Pd clusters with 13, 55, 147 atoms are examples. The geometry of these extremely small clusters with unique minimum energy has been extensively studied[14,26]. In this work, we pay attention to the time evolution of the structures during heating by investigating two parameters: atomic number distribution on z direction and bond order parameters.

The atomic number distribution *N(z)* for each element is defined as

$$N(z) = \left\langle \sum_i \delta(z_i - z) \right\rangle \tag{6}$$

N(z) is a good way to look at the structural features during heating of spherical cluster and one dimensional nanowire of similar diameter. Plots in Figure 6 describe the distribution of Pd atoms along *z* axis (nanowire axis) at different temperatures. In the solid phase, atoms have higher distribution only at certain distances from the center, forming many sharp peaks. Those

peaks become wider and shorter upon heating, and finally disappear due to the uniformly distributed atoms in liquid phase. This expected behavior in *N(z)* is seen in the Pd cluster case, as shown in Figure 6(a). In contrast, Figure 6(b) for the nanowire exhibits complicated structural features. This distribution shows two main shapes before melting. Below 1100K, *N(z)* shows three peaks in the middle and two ends as shown for 600K in Figure 6(b). It is easy to see that the Pd nanowire is trying to form a ball shape and have a repetitive distribution unit as the one shown for the cluster. It also indicates that perfect crystalline structure is not stable in a thin nanowire case even at this lower temperature. The nature of the distribution curve changes for temperatures above 1100K, with the middle peak disappearing. Just below the melting temperature of 1200 K, the middle part of the nanowire shows almost even density distribution, characteristic of a liquid. This, we may interpret as a tendency of necking of the wire before breaking. Simulations of much longer wires over longer simulation times would confirm these mechanical instabilities.

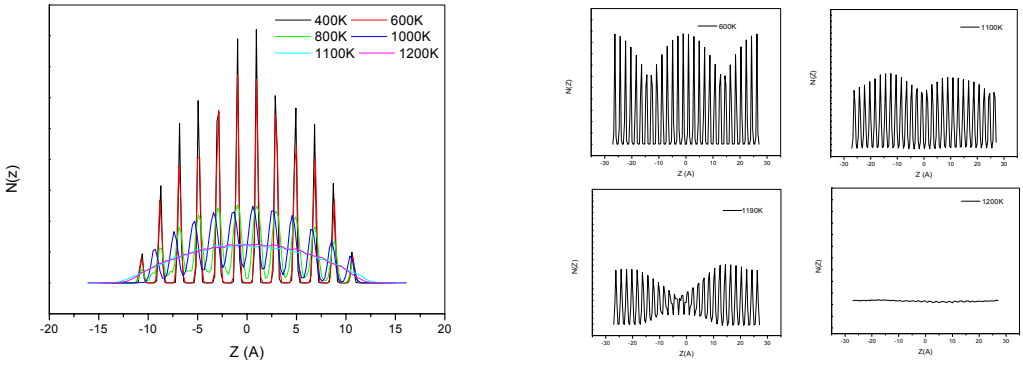

FIG. 6. Comparison of Pd atomic distributions of (a) Pd cluster (right) and (b) Pd nanowire (right) along a Cartesian coordinate (z) at different temperatures.

The bond order parameters (BOP) method [39] was applied to quantify structural evolution of the clusters and nanowries crystallographically, as well as to distinguish between liquid-like and solid-like states. Bonds are defined as the vectors joining a pair of neighboring atoms with an interatomic distance less than a specified cutoff radius. The cutoff distance is usually chosen as the position of the first minimum in the pair correlation function, which is about 3.36 Å is this case. Associated with every bond are a set of numbers called local bond order parameters:

$$Q_{lm}(r) = Y_{lm}\left(\theta(r), \phi(r)\right), \tag{7}$$

where $Y_{lm}(\theta,\phi)$ are spherical harmonics and $\theta(r)$ and $\phi(r)$ are the polar angle and azimuthal angles of vector r with respect to an arbitrary reference frame. Only even-*l* spherical harmonics are considered, which are invariant under inversion. A global bond order parameter $\bar{Q}_{lm}(r)$ can be defined by averaging $Q_{lm}(r)$ over all bonds in the system:

$$\bar{Q}_{lm} = \frac{1}{N_b}\sum Q_{lm}(r), \tag{8}$$

where N_b is the number of bonds. To let $\bar{Q}_{lm}(r)$ not depend on the choice of reference frame, a second-order invariant is constructed as:

$$Q_l = \left(\frac{4\pi}{2l+1} \sum \left| \bar{Q}_{lm} \right|^2 \right)^{1/2}, \quad (9)$$

and a third-order invariant is constructed as:

$$W_l = \sum_{m1,m2,m3} \begin{pmatrix} l & l & l \\ m_1 & m_2 & m_3 \end{pmatrix} \bar{Q}_{lm_1} \bar{Q}_{lm_2} \bar{Q}_{lm_3} . \quad (10)$$

The term in the bracket is a Wigner-3j symbol.[40] Furthermore, a reduced order parameter $\hat{W}_l$ is defined so that it is not sensitive to the precise definition of the nearest neighbor of a particle:

$$\hat{W}_l = W_l / \left(\sum \left| \bar{Q}_{lm} \right|^2 \right)^{3/2} . \quad (11)$$

The values of these bond order parameters for some common crystal structures are listed in Table 2.

TABLE 2 Bond order parameters for a number of simple cluster geometries[39]

Geometry	Q_4	Q_6	$\hat{W}_4$	$\hat{W}_6$
Icosahedra	0	0.66332	0	0.16975
Fcc	0.19094	0.57452	0.15932	0.01316
Hcp	0.09722	0.48476	0.13410	0.01244
Bcc	0.03637	0.51069	0.15932	0.01316
Liquid	0	0	0	0

Because of symmetry, the first nonzero values occur for *l=4* in the cluster with cubic symmetry and for *l*=6 in clusters with icosahedral symmetry. We used the four bond order parameters $Q_4, Q_6, \hat{W}_4, \hat{W}_6$ together to identify structures. Note that Q is of the same order of magnitude for all crystal structures of interest, which makes it less useful for distinguishing different crystal structures compared to $\hat{W}$. But Q_6 is useful to identify phase transitions, since it has a larger value than other parameters and decrease quickly to zero when the system becomes liquid.

Considering the surface effect in nanomaterials and to get more accurate answers to monitor global structural changes, we calculated bond order parameters for internal atoms, surface atoms and all atoms in the systems. We find out that only the second-order invariants (Q values) slightly differ when the surface atoms are excluded, while the third-order invariants ($\hat{W}$ values) are not affected. This is because Q is more sensitive to the number of the nearest neighbors. Therefore we use BOP for the entire system. Figure 7 shows the bond order parameter comparison between the entire Pd cluster and the Pd nanowire. All the parameters drop abruptly to zero at the transition temperature. These changes are more obvious in Q_6. Even though the Pd cluster retains the fcc structure at lower temperatures, the time averaged global bond order parameters show that the Pd nanowire moves away from the starting fcc structure. The correlation plot for $\hat{W}_6$ as a function of Q_6 is shown in Figure 8, where the red dots are the values for perfect crystals. We use Q_6 because it changes significantly with temperature. We see from the time averaged bond order parameters that the nanowire move

closer hexagonal close-packed (hcp) structure, from its initial fcc structure, at all solid-like temperatures below the transition point.

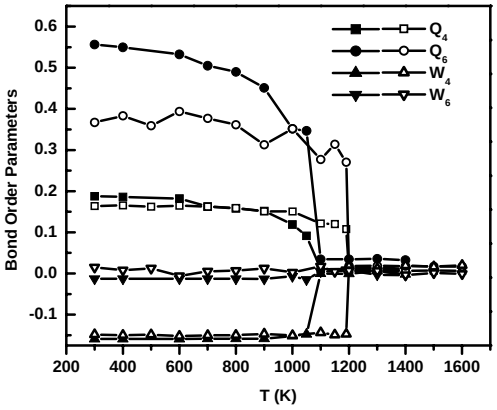

FIG. 7. Temperature dependence of average bond order parameters for the Pd cluster with 456 atoms and Pd nanowire with 1568 atoms during heating. Filled and unfilled symbols represent cluster and nanowire, respectively.

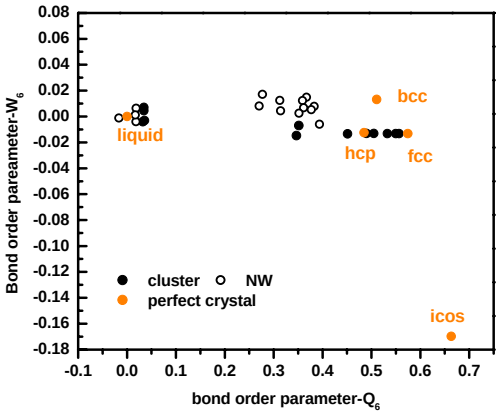

FIG. 8. Correlation plot for bond order parameters W_6 as a function of Q_6

4. Conclusions

The simulation studies of this work indicate that a 2.3 nm diameter Pd nanowire has lower melting temperature than Pd bulk but higher than the same diameter Pd cluster. Both Pd nanowires and nanoclusters exhibit surface pre-melting, the structural and dynamical nature of which is somewhat different. These differences are fully characterized by several thermodynamic, structural and dynamic variables in this study. The general picture that emerges is that the surface pre-melting behavior for the cluster is similar to that of other noble and transition metal nanoclusters. The nanowire exhibits a higher pre-melting temperature range, and dynamical behavior characterized by increased movement of atoms in the plane perpendicular to the axis followed by increased movement across these planes, as the temperature approaches the transition temperature. A quasi-liquid skin grows from the surface in the radial direction for both cluster and wire, in the surface pre-melting regime, followed by the breakdown of order in the remaining solid core at the transition temperature. Bond order parameters indicated that the cluster retained the initial fcc structure, whereas, the nanowire tended towards the hcp structure. Projected density profiles indicated that the nanowire could undergo mechanical instabilities and break upon heating. Simulations of longer as well as different diameter clusters and nanowires of Pd are suggested by this work for a complete understanding of the mechanical behavior as well as melting transitions.

Acknowledgement

Partial support was provided by NASA-Glenn via FSEC, Florida. The Daresbury Laboratory provided the DL_POLY package and Academic Computing at the University of South Florida provided computational resources, both of which are gratefully acknowledged. The authors thank Subramanian K.R.S.S. for some valuable discussions.

Reference

* Electronic address: bhethana@eng.usf.edu

1 M. Schmidt *et al*., Phys.Rev.Lett.**79**, 99 (1997).
2 F. Ercolessi, W. Andreoni, and E. Tosatti, Phys. Rev. Lett. **66**, 911 (1991).
3 M. Schmidt *et al*., Nature **393**, 238 (1998).
4 S. L. Lai et al., Phys. Rev. Lett. **77**, 99 (1996).
5 K. F. Peters, J. B. Cohen, and Y-W Chung, Phys. Rev. B **57**, 13430 (1998).
6 R. R. Couchman, Phil. Mag. A **40**, 637 (1979).
7 R. C. Longo, Surf. Sci. **459**, L441 (2000).
8 T. X. Li, Y. L. Ji, S. W. Yu, and G. H. Wang, Solid State Comm. **116**, 547 (2000).
9 C. Rey *et al*., Phys. Rev. B **48**, 8253 (1993).
10 Y Shimizu, K. S. Ikeda, and S. Sawada, Phys. Rev. B **64**, 075412 (2001).
11 S-P. Huang, and P. B. Balbuena, J. Phys. Chem.B **106**, 7225 (2002).
12 Y. G. Chushak, and L. S. Bartell, J. Phys. Chem. B **105**, 11605 (2001).
13 B. Wang, G. Wang, X. Chen, and J. Zhao, Phys. Rev. B **67**, 193403 (2003).
14 C. L. Cleveland, W. D. Luedtke, and U. Landman, Phys. Rev. B **60**, 5065 (1999).
15 F. Ercolessi, W Andreoni, and E. Tosatti, Phys. Rev. Lett. **66**, 911 (1991).
16 O. Gülseren, F. Ercolessi, and E. Tosatti, Phys. Rev. B **51**, 7377 (1995).
17 H. B. Liu, J. A. Ascencio, M. P. Alvarez, and M. J. Yacaman, Surf. Sci. **491**, 88 (2001).
18 J. Wang *et al*., Phys. Rev. B **66**, 085408 (2002).
19 G. Schmid *et al*.; J. Mol. Catal. A **107**, 95 (1996).
20 H-U. Blaser, J. Mol. Catal. A **173, 3.** (2001).
21 F. Favier *et al*., Science. **293**, 2227 (2001).
22 E. C. Walter, Surface and Intersurface Analysis. **34**, 409 (2002).
23 J. Kong, M. Chapline, and H. Dai, Adv. Mater. **13**, 1384 (2001).
24 G. Schmid *et al*., Chemical Society Reviews. **28,** 179 (1999).
25 Y. Volokitin *et.al*., Nature. **384**, 621 (1996).
26 J. Westergren and S. Nordholm, Chem. Phys. **290**,189 (2003).
27 A. P. Sutton, and J. Chen, Phil. Mag. Lett. **61**,139 (1990).
28 J Uppenbrink, and D. J. Wales, J. Chem. Phys. **98**, 5720 (1993).
29 D. J. Wales, and L. J. Munro, J. Phys. Chem. **100**, 2053 (1996).
30 L. D. Lloyd and R. L. Johnston, Dalton **3**, 307 (2000).
31 Z. A. Kaszkur and B. Mierzwa, Phil. Mag. A **77**, 781 (1998).
32 J. A. Nieminen, Phys. Rev. Lett. **74**, 3856 (1995).
33 W. Smith, and T. R. Forester, DL_POLY; Daresbury Laboratory, Daresbury, UK,1996.
34 M. P. Allen, and D. J. TIldesley, Computer simulation of liquids, Clarendon Press, Oxford, 1987.
35 L. Wang, Y. Zhang, X. Bian, and Y. Chen, Phys. Lett. A **310**, 197 (2003).
36 Y.Qi, T. Çağin, W. L. Johnson, and W. A. Goddard, J. Chem. Phys. **115**, 385 (2001).
37 F. Calvo, and F. Spiegelmann, J. Chem. Phys. **112**, 2888, (2003).
38 O. Echt, K. Sattler and E. Recknagel, Phys. Rev. Lett, **47**, 1121 (1981).
39 P. J. Steinhardt, D. R. Nelson and M. Ronchetti, Phys. Rev. B **28**, 784 (1983).
40 J. J.Sakurai *Modern Quantum Mechanics* (Addision-Wesley, 1994), Rev.Ed., p.200.